Astron. Astrophys. 355, 512–524 (2000)

ASTRONOMY AND ASTROPHYSICS

The interstellar medium in the edge-on galaxy NGC 5907

Radio continuum emission and magnetic fields

M. Dumke[1,2], **M. Krause**[1], **and R. Wielebinski**[1]

[1] Max-Planck-Institut für Radioastronomie, Auf dem Hügel 69, 53121 Bonn, Germany
[2] Institut de Radio Astronomie Millimétrique, 300 rue de la Piscine, 38406 St. Martin d'Hères, France

Received 21 October 1999 / Accepted 16 November 1999

Abstract. We observed the non-interacting edge-on galaxy NGC 5907 in total power and polarized radio continuum emission at wavelengths of $\lambda\lambda$ 2.8, 6.2, and 20 cm, using the VLA and the Effelsberg 100-m telescope.

The total power emission of the galaxy shows (after subtraction of a double background source in the southern half) its maximum intensity slightly shifted to the north with respect to the optical and dynamical centre. The high spatial resolution of the 20 cm data allows to distinguish two emission components, a thin and a thick disk, with scale-heights of 0.34 and 1.5 kpc respectively at this wavelength. The spectral indices over the observed frequency range suggest a thermal fraction of the emission much larger than usually assumed for normal galaxies, more than 70 % at λ 2.8 cm. This finding is further supported by the spectral index distribution in the disk and the very weak polarization, which does not exceed $\sim 15\,\%$. From the estimated thermal (free-free) emission we calculated an averaged thermal electron density in the ISM of NGC 5907 of $n_{\rm e} \sim 0.03\,{\rm cm}^{-3}$ (for a clumping factor $f = 20$), a value similar to the local interstellar medium.

From the nonthermal and the polarized intensity on the major axis we could estimate the total magnetic field strength in NGC 5907 to $B_{\rm tot} \sim 5\,\mu$G. We found some evidence that the large-scale component of the total field is aligned with the galactic plane, as in most other galaxies, but is relatively weak ($B_{\rm u} \sim 1.1\,\mu$G). This weakness of the large-scale magnetic field and the small nonthermal fraction of the radio continuum emission at high frequencies can easily explain the non-detection of polarized emission at λ 2.8 cm.

When we compare our results with previous ones on the radio continuum emission in nearby galaxies, we find that the quiescent galaxy NGC 5907 (in terms of star formation) is characterized by a deficiency of nonthermal radio emission. Hence we argue that in general a higher star formation activity, as observed in some other galaxies, may lead to a proportional enhancement of the thermal free-free emission from H II regions, but – with some time lag – to a much more significant increase of the number density of relativistic electrons and a more effective amplification of the large-scale magnetic field, and therefore to a higher amount of nonthermal (synchrotron) radiation from those more actively star-forming galaxies than from the rather inactive galaxy NGC 5907.

Key words: galaxies: individual: NGC 5907 – galaxies: ISM – galaxies: magnetic fields – galaxies: spiral – radio continuum: galaxies – polarization

Send offprint requests to: M.Dumke (mdumke@mpifr-bonn.mpg.de)

1. Introduction

Ongoing star formation in the disk of a spiral galaxy and subsequent supernova explosions of massive stars lead to an enrichment of the surrounding interstellar medium with thermal and relativistic electrons. Their spatial and energy distribution is strongly connected not only to the star forming activity in this galaxy and the distribution and the amount of available raw material, i.e. molecular and atomic hydrogen, but also to the strength and morphology of uniform and random magnetic fields in the vicinity of the electron-producing regions.

Radio continuum observations of external galaxies at cm-wavelengths provide a considerable amount of information about the relativistic electrons themselves and the properties of magnetic fields in these objects. The spectral behaviour of the observed radiation tells us about the energy distribution of the emitting electrons and also about the emission mechanism (thermal or non-thermal). The observed degree of linear polarization gives us the opportunity to study the uniformity of the magnetic field, the typical correlation lengths and the depolarization mechanisms. The orientation of the observed polarization vectors at different wavelengths additionally allows us to determine the intrinsic magnetic field orientation and the properties of the Faraday-active magneto-ionic medium along the line-of-sight.

The nearby spiral galaxy NGC 5907, classified as Sc (de Vaucouleurs et al. 1991), is one of the largest edge-on systems visible on the sky. Its distance is about 11 Mpc (Sasaki 1987), its inclination $86\overset{\circ}{.}5$ (García-Burillo et al. 1997). With an infrared luminosity of $L_{\rm IR} = 7.5\,10^9\,L_\odot$ (Young et al. 1989, corrected to $D = 11\,{\rm Mpc}$) it is an infrared-weak and therefore only moderately star-forming galaxy, compared to other isolated galaxies already investigated in the cm range, e.g. NGC 891. Neverthe-

less NGC 5907 received some attention in the past due to several interesting findings. Already more than twenty years ago it was the first (presumed) non-interacting galaxy where an H I warp was detected (Guélin et al. 1974; Sancisi 1976). More recently a luminous stellar halo was found, with a light distribution which may trace the dark matter in this galaxy (Sackett et al. 1994; Lequeux et al. 1996). New optical observations (Lequeux et al. 1998; Shang et al. 1998) suggest a past interaction between NGC 5907 and a neighbouring elliptical or dwarf galaxy. Concerning the neutral ISM in the disk, molecular gas was observed by García-Burillo et al. (1997), who found a nuclear molecular bar in this galaxy, and by Dumke et al. (1997) who investigated the distribution of the molecular gas on larger scales, and its interplay with atomic hydrogen and dust.

The radio continuum emission of NGC 5907 was observed by Hummel et al. (1984) at $\lambda\lambda\,21$ and 49 cm and by Dumke et al. (1995) at $\lambda\,2.8$ cm, who compared the radio properties of several nearby galaxies. In contrast to the other objects in their sample, they detected no polarized emission in NGC 5907. Up to now the reason for this was not clear, especially given that some properties of this galaxy are similar to those of other normal (i.e. moderately star-forming) galaxies, e.g. NGC 4565.

The present paper gives a deeper analysis of the radio continuum emission of this galaxy. New data were obtained during observations with the VLA and the Effelsberg radio telescope, which will be described in the following section. Sect. 3 will then present the results at the different wavelengths, and in Sect. 4 we will analyse and discuss the data to investigate the properties of the ISM in NGC 5907. In the final section, we will draw some conclusions and summarize our results.

Some basic parameters that we adopt for NGC 5907 are given in Table 1; all astronomical coordinates in this paper are in B(1950.0).

Table 1. Some basic parameters of NGC 5907

Type	Sc	(de Vaucouleurs et al. 1991)
Dynamical centre:		(García-Burillo et al. 1997)
R.A. [1950]	$15^{\rm h}14^{\rm m}35\overset{\rm s}{.}5$	
Dec. [1950]	$56^\circ30'43\overset{''}{.}3$	
$v_{\rm hel}$	677 km/s	(García-Burillo et al. 1997)
R_{25}	19.7 kpc	
Distance	11 Mpc	(Sasaki 1987)
	($1''$ corresponds to 53 pc)	
$L_{\rm IR}$	$7.5\,10^9\,L_\odot$	(Young et al. 1989)
Pos. Angle	155°	(Barnaby & Thronson 1992)
Incl.	86.5°	(García-Burillo et al. 1997)

2. Observations and data reduction

2.1. VLA observations

The observations around $\lambda\,20$ cm were made with the Very Large Array (VLA) of the NRAO[1]. They were carried out on March 28th, 1991 with a total observing time of 11 hrs, using two IFs centered on 1465 MHz and 1665 MHz with a bandwidth of 50 MHz each. We used the D configuration with a longest spacing of 1.0 km and a shortest spacing of 40 m. As the field centre we took $\mathrm{R.A.}[1950] = 15^{\rm h}15^{\rm m}0$, $\mathrm{Dec.}[1950] = 56^\circ30'0$.

The calibration of the data was performed by the NRAO staff using the sources 3C286 and 1437+624 as calibrators. The subsequent data reduction was done with the standard AIPS program package of the NRAO in a usual manner. A first cleaned map showed systematic distortions in the background due to a strong point source $25'$ southwest of the phase centre, at $\mathrm{R.A.}[1950] = 15^{\rm h}16^{\rm m}07\overset{\rm s}{.}4$, $\mathrm{Dec.}[1950] = 56^\circ07'30\overset{''}{.}6$. We used the CLEAN components of this source to create model visibilities and subtract them from the uv data set in the Stokes parameter I. In polarization the effect of this source was negligible. To further improve the data quality, the uv data have been self-calibrated for the phase. An attempt to self-calibrate for the amplitude did not lead to better results. Final maps of the Stokes parameters I, U and Q were produced with a clean beam of $41''$ $HPBW$. Finally we applied a primary beam correction to the resulting maps in total and polarized intensity. The rms noise around the field centre reaches values of 80 μJy/beam in total power and 35 μJy/beam in polarization.

[1] The NRAO is a facility of the National Science Foundation operated under cooperative agreement by Associated Universities, Inc.

2.2. Effelsberg observations

The observations at 4.85 GHz ($\lambda\,6.2$ cm) were made in July and August 1996 with the 2-horn receiver system available at the Effelsberg 100-m telescope of the MPIfR. Each horn is equipped with two total power amplifiers and an IF polarimeter, similar to the 10.55 GHz receiver system. The bandwidth is 500 MHz, the system noise temperature about 28 K, and the resolution is $147''$ ($HPBW$) at 4.85 GHz.

For pointing, focussing and calibration at this wavelength we observed regularly the sources 3C286, 3C295, NGC 7027 and 2234+28. We obtained a total of 27 coverages, which led, after restoration (Emerson et al. 1979) and combination (Emerson & Gräve 1988), to an rms noise in the final maps of $400\,\mu$Jy/beam in total power and $80\,\mu$Jy/beam in polarization.

To remove the sidelobes of the antenna pattern and to improve the dynamical range we applied a new CLEANing method described briefly in Rottmann et al. (1996). For this purpose we used two maps of 3C84 observed in summer 1996 as antenna patterns. Using a procedure developed by Rottmann (1996), we were also able to reduce the instrumental polarization caused by the antenna responses for Stokes Q and U down to level of 0.3 %.

The observations at 10.55 GHz ($\lambda\,2.8$ cm) were performed between April and July 1992 with the Effelsberg 100-m telescope. The receiver system, the observations, and the data reduction were already described in Dumke et al. (1995). In the final radio maps at $\lambda\,2.8$ cm we obtained noise values of $500\,\mu$Jy/beam in total power and $290\,\mu$Jy/beam in polarization. The $HPBW$ of the telescope at this wavelength is $69''$.

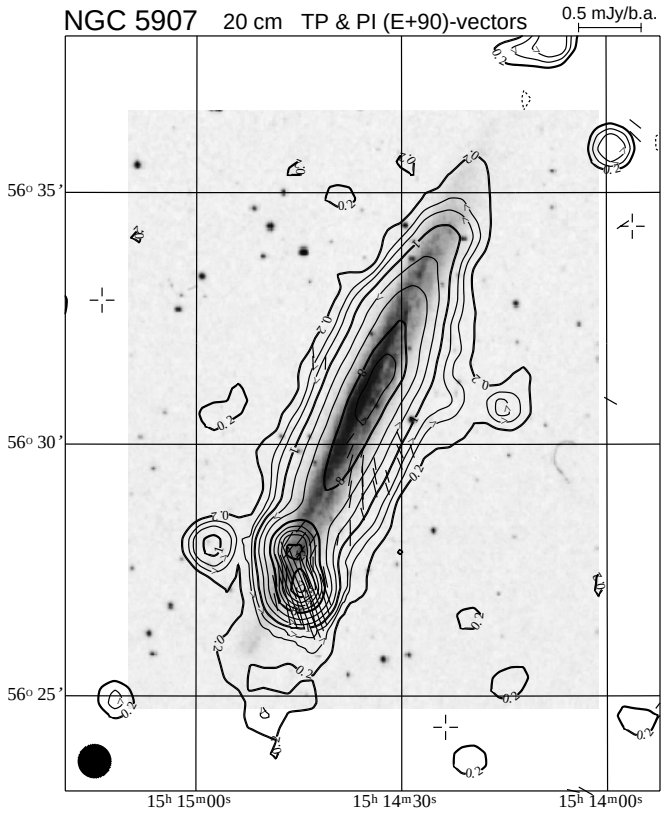

Fig. 1. Contour map of the total intensity at $\lambda\,20$ cm, overlaid on an optical image. The rms noise is $80\,\mu\mathrm{Jy/beam}$, the beam is $41''$ as indicated by the hatched circle in the lower left corner. Contour levels are -0.2 (dashed), 0.2, 0.4, 0.6, 1, 2, 4, 8, 12, 16, 20, 25, 30 mJy/beam. Vectors indicate the orientation of the E-vectors, rotated by $90°$; their lengths are proportional to the polarized intensities. $1'$ corresponds to 0.4 mJy/beam. Vectors are only plotted if $PI \geq 0.1$ mJy/beam. Coordinates are in B(1950.0)

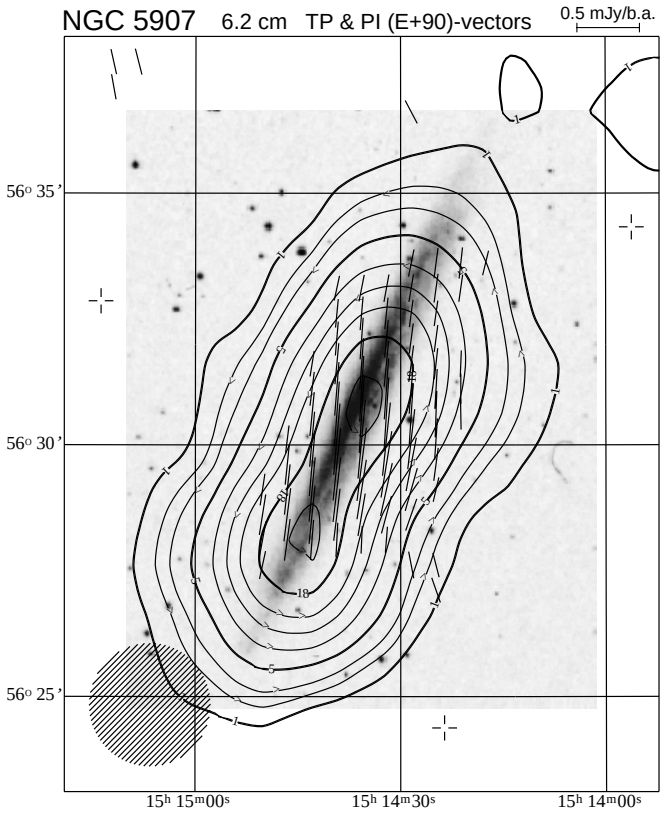

Fig. 2. Contour map of the total intensity at $\lambda\,6.2$ cm, overlaid on an optical image. The rms noise is 0.4 mJy/beam, the beam is $147''$ as indicated by the hatched circle in the lower left corner. Contour levels are 1, 2, 3, 5, 8, 11, 14, 18, 22 mJy/beam. Vectors indicate the orientation of the E-vectors, rotated by $90°$; their lengths are proportional to the polarized intensities. $1'$ corresponds to 0.4 mJy/beam. Vectors are only plotted if $PI \geq 0.2$ mJy/beam. Coordinates are in B(1950.0)

3. Results

3.1. The total intensity maps

3.1.1. NGC 5907 at 20 cm

Fig. 1 shows the total intensity map obtained with the VLA at $\lambda\,20$ cm, overlaid on an optical image extracted from the Digitized Sky Survey. An outstanding feature in this map is the double source in the southern half of the galaxy. The spectral behaviour of this double source (see further below), its non-variable nature (see e.g. Hummel et al. 1984) and also the non-zero probability of finding a radio source as strong as this within the extent of a galaxy on the sky suggest that this double source is a background source projected onto the southern half of NGC 5907. Two more background point sources are also visible in the direct vicinity of the galaxy. The galaxy itself is asymmetric: at lower intensities, the radio continuum emisssion is more extended to the south than to the north, while the maximum intensity is shifted several arcsec to the north (see also Fig. 8).

Also shown in Fig. 1 is the polarized intensity in the form of polarization (E-field) vectors, rotated by $90°$. Note that due to possible Faraday rotation effects in the galaxy itself and between the galaxy and the observer at this wavelength the $(E + 90)$-vectors do not necessarily indicate the intrinsic magnetic field orientation as is the case at (much) shorter wavelengths.

3.1.2. NGC 5907 at 6.2 cm

The total intensity map at $\lambda\,6.2$ cm is shown in Fig. 2. Because of the limited resolution of the Effelsberg telescope at this wavelength ($147''$), none of the point sources in the vicinity of NGC 5907 that are visible in the 20 cm map could be distinguished from the galaxy's emission. However, the double background source in the southern half could be identified as a second emission maximum south of the centre of NGC 5907. In general the distribution of the emission seems to be similar to that at $\lambda\,20$ cm wavelength.

Also shown are the $(E + 90)$-vectors whose lengths are proportional to the polarized intensity. They will be described in the next subsection.

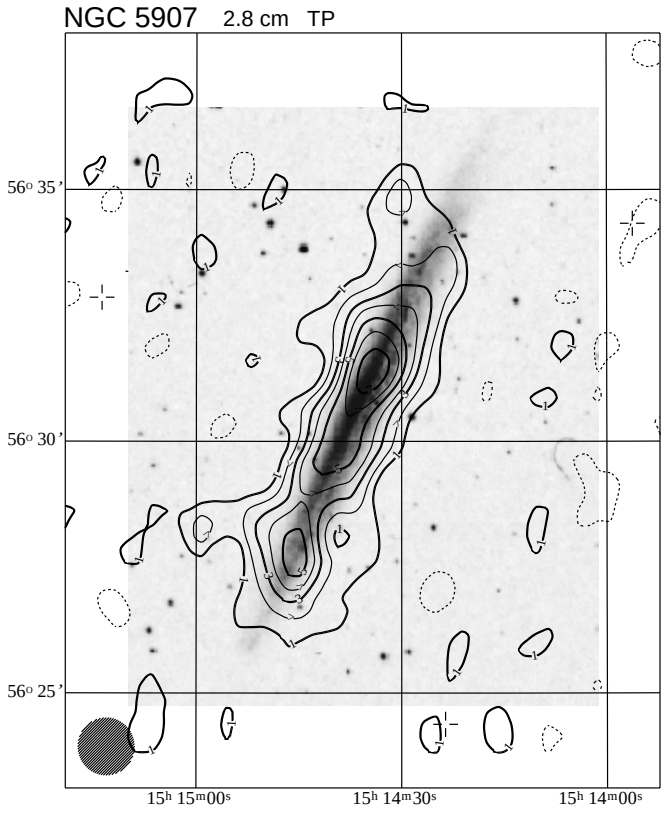

Fig. 3. Contour map of the total intensity at $\lambda\,2.8\,\mathrm{cm}$, overlaid on an optical image. The rms noise is 0.5 mJy/beam, the beam is $69''$ as indicated by the hatched circle in the lower left corner. Contour levels are -1 (dashed), 1, 2, 3, . . . , 7 mJy/beam. Coordinates are in B(1950.0)

3.1.3. NGC 5907 at 2.8 cm

Although the sensitivity of the 2.8 cm data is below that of the 6.2 cm data (and therefore the S/N-ratio much lower), the better resolution available at $\lambda\,2.8\,\mathrm{cm}$ with the Effelsberg telescope offers a deeper insight into the structure of the radio continuum emission. The radio map obtained at this wavelength – which is identical to Fig. 5 in Dumke et al. (1995) – is shown, overlaid on an optical image, in Fig. 3. Besides the double source in the southern half, the background point source southeast of the galaxy is also visible. As at 20 cm, an asymmetry of the emission is detected also at 2.8 cm in the sense that the maximum intensity seems to be shifted to the north.

3.2. Total flux densities

Using a ring integration method, we determined total flux densities of NGC 5907 from the final maps. At $\lambda\,20\,\mathrm{cm}$ we get $S_{20\mathrm{cm}} = 180 \pm 12\,\mathrm{mJy}$, *including* the contribution of the double source in the southern half. Hummel et al. (1984) estimated a value of $157 \pm 15\,\mathrm{mJy}$, which is below our value, but still consistent with it within the errors. Moreover, our value may be rather a lower limit because the amount of non-detected flux due to missing spacings is not known, although a check of the zero level in our map doesn't yield any evidence for lost flux.

At $\lambda\,6.2\,\mathrm{cm}$, the flux determination is not as straightforward since the emission of the background point sources in the direct vicinity of NGC 5907 cannot be separated from the galaxy's emission due to the large telescope beam. In a first order approximation, however, our flux density estimate of $S_{6.2\mathrm{cm}} = 74 \pm 6\,\mathrm{mJy}$ is sufficiently accurate because it is consistent with previous flux density values found in the literature (Hummel et al. 1984, and references therein).

For $\lambda\,2.8\,\mathrm{cm}$ we find $S_{2.8\mathrm{cm}} = 47 \pm 5\,\mathrm{mJy}$, also including the background sources in the direct vicinity of NGC 5907.

3.2.1. The integrated radio spectrum

Dumke et al. (1995) investigated the radio continuum spectrum of NGC 5907, using measurements from 327 MHz up to 10.55 GHz, and found, assuming a single power law spectrum, a radio spectral index of $\alpha = -0.79 \pm 0.03$ ($S_\nu \propto \nu^\alpha$). With the new data points at 20 and 6.2 cm (and excluding those older than 25 years) we find a value of $\alpha = -0.78 \pm 0.06$, hence no difference to the older value. There is, however, strong evidence that the total flux density spectrum cannot be described by only one component: Hummel et al. (1984) found a spectral index of $\alpha = -0.9 \pm 0.1$ for $\nu \leq 1410\,\mathrm{MHz}$ and a flatter spectrum with $\alpha = -0.6 \pm 0.1$ for $\nu \geq 1410\,\mathrm{MHz}$. Niklas et al. (1997) separated the thermal and nonthermal radio emission for a large sample of spiral galaxies and found for NGC 5907 a nonthermal spectral index of $\alpha_{\mathrm{nth}} = -1.05$ and a very large thermal fraction of $\mathrm{f_{th}}(2.8\,\mathrm{cm}) = 63\,\%$ for the total emission. These findings make it worth studying the spectral behaviour of NGC 5907 in more detail. We therefore separate in the following the galaxy emission from the emission of the background sources.

3.2.2. Point sources in the southern half of NGC 5907

From the data at $\lambda\lambda$ 20 and 2.8 cm we can (due to the high spatial resolution) determine the accurate positions and flux densities of the point sources around NGC 5907. Even if it cannot be ruled out that the point sources in the southern half belong to the galaxy itself, their intensities at the various wavelengths exhibit a different spectral behaviour than that of the galaxy, so it is necessary to remove these sources from the maps if we want to discuss the emission of the galaxy.

Table 2 lists the determined parameters of the two point sources. The positions and flux densities were also estimated by Hummel et al. (1984) at frequencies of 1410 MHz and 610 MHz. These positions show small deviations from our values which may be due to difficulties in subtracting these sources because of the lower resolution of their data. Nevertheless the spectral indices found by these authors agree within the errors with those listed in Table 2. This lack of variation of the spectral index with frequency enables us to subtract these sources, properly scaled to the larger beam, also from the $\lambda\,6.2\,\mathrm{cm}$ map. The calculated flux densities of the point sources at this wavelength are 8.1 mJy (S1) and 7.5 mJy (S2).

Table 2. Estimated parameters of the point sources in the southern half of NGC 5907

Source	Position		Flux Densities [mJy]		Spectral index	Polarization	
	R.A.[1950]	Dec.[1950]	$S_{20\mathrm{cm}}$	$S_{2.8\mathrm{cm}}$	$\alpha_{20/2.8}$	$p_{20\mathrm{cm}}$ [%]	$\chi_{20\mathrm{cm}}$ [°]
NGC5907-S1	$15^{\mathrm{h}}14^{\mathrm{m}}45\overset{\mathrm{s}}{.}75 \pm 0\overset{\mathrm{s}}{.}10$	$56°27'56\overset{''}{.}0 \pm 1\overset{''}{.}0$	26.5 ± 2.0	3.6 ± 0.5	-1.05 ± 0.07	—	—
NGC5907-S2	$15^{\mathrm{h}}14^{\mathrm{m}}44\overset{\mathrm{s}}{.}76 \pm 0\overset{\mathrm{s}}{.}08$	$56°27'08\overset{''}{.}4 \pm 0\overset{''}{.}8$	31.0 ± 1.5	2.8 ± 0.5	-1.26 ± 0.09	2.3 ± 0.3	114 ± 2

3.3. Polarized intensity

Fig. 4 shows the polarized intensity at λ 20 cm, as measured with the VLA. Polarization could basically be detected in the southwestern part of NGC 5907. The maximum in the polarized intensity map is due to the source NGC5907-S2, which has a total polarized flux density of $0.7 \pm 0.1\,\mathrm{mJy}$, a degree of polarization of $2.3 \pm 0.3\,\%$ and a polarization angle of $114° \pm 2°$. The source NGC5907-S1 may also be polarized, but in that case its polarized emission cannot be distinguished from that of the galaxy at the corresponding position and is therefore neglected here. Due to the orientation of the galaxy which is not perfectly edge-on ($i = 86\overset{\circ}{.}5$) the distribution of the linearly polarized emission can be qualitatively explained by different pathlengths of the radiation from the southwestern and the northeastern half. Since the southwestern half represents the front side of the galaxy (this is suggested by the location of the dust lane visible on optical images), the polarized emission from this region is probably not strongly affected by any depolarizing medium in the galaxy itself. The emission from the rear side (the northeastern one), however, has to pass through some Faraday active medium and may therefore be completely depolarized at this wavelength. To explain the observed asymmetry with respect to the minor axis, on the other hand, some non-axisymmetric features are necessary, but they can be provided easily by the spiral structure and its consequences, like different magnetic field morphology or different physical properties of the ISM.

The polarized flux density of NGC 5907 excluding the source S2 is $S_{PI,20\mathrm{cm}} = 1.8 \pm 0.3\,\mathrm{mJy}$, yielding an overall degree of polarization at this wavelength of $p_{20\mathrm{cm}} = 1.5 \pm 0.3\,\%$. We should note, however, that the 20 cm map of the polarized intensity was produced using the combined data from both IFs. In fact Faraday rotation may occur between these two wavelengths and lead to some additional depolarization (see Sect. 4.6). The PI-maps for the two individual IFs are shown in Fig. 9.

The polarized emission detected with the Effelsberg telescope at λ 6.2 cm is shown in Fig. 5. The maximum of PI is located somewhat south of the central position and reaches valus of about 0.6 mJy/beam. Similar to the situation at λ 20 cm, the polarized emission is strongest in the southwestern part, but is also, at the first contour level, extended to the northern half of the galaxy. The southern point source S2, however, seems to be completely depolarized at this wavelength. Since Faraday depolarization effects are expected to be stronger at longer wavelengths, this missing polarized emission is most probably due to wavelength-independent beam depolarization within the larger beam of the Effelsberg telescope, and different polarization angles of the source S2 and the southernmost part of NGC 5907.

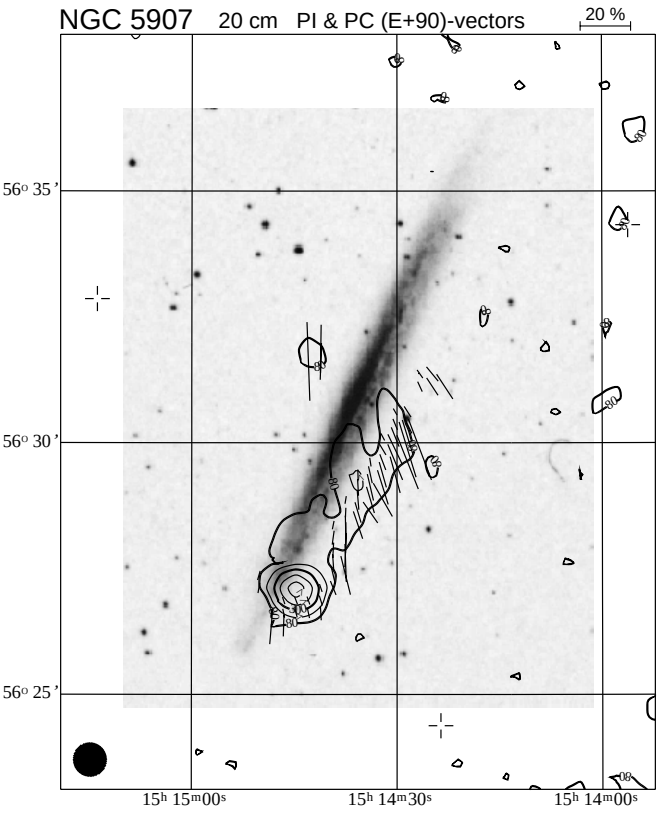

Fig. 4. Contour map of the polarized intensity at λ 20 cm, overlaid on an optical image. The rms noise is $35\,\mu\mathrm{Jy/beam}$, the beam is $41''$ as indicated by the hatched circle in the lower left corner. Contour levels are 80, 160, 300, 500, 700 μJy/beam. Vectors indicate the orientation of the E-vectors, rotated by 90°; their lengths are proportional to fractional polarizations. $1'$ corresponds to 20 %. Vectors are only plotted if $p \geq 3\,\%$. Coordinates are in B(1950.0)

The integrated polarized flux density at λ 6.2 cm, as obtained by integrating over the map, is $S_{PI,6.2\mathrm{cm}} = 1.4 \pm 0.2\,\mathrm{mJy}$. After subtracting the two background sources S1 and S2 from the total intensity map, this yields an integrated degree of polarization of $p_{6.2\mathrm{cm}} = 2.4 \pm 0.5\,\%$. As expected, this value is larger than $p_{20\mathrm{cm}}$ because of smaller Faraday depolarization effects. Interesting enough, the value for $p_{20\mathrm{cm}}$ does not change significantly when estimated from maps that are smoothed to $147''$ *HPBW* (the resolution of the 6.2 cm data). This means that the so-called "beam depolarization", which is due to changing orientations of the polarization vectors within the telescope beam, does not change on spatial scales between $\sim 2.2\,\mathrm{kpc}$ (corresponding to an angular resolution of $41''$) and $\sim 7.8\,\mathrm{kpc}$ (corresponding to $147''$). Hence the magnetic fields which we refer to as "turbu-

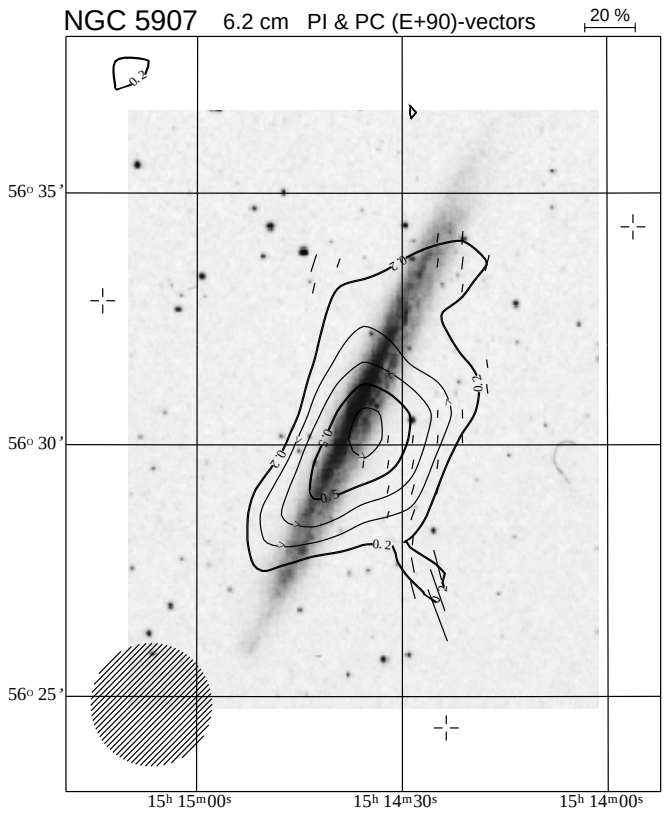

Fig. 5. Contour map of the polarized intensity at λ 6.2 cm, overlaid on an optical image. The rms noise is $80\,\mu\mathrm{Jy/beam}$, the beam is $147''$ as indicated by the hatched circle in the lower left corner. Contour levels are 200, 300, ..., 600 μJy/beam. Vectors indicate the orientation of the E-vectors, rotated by $90°$; their lengths are proportional to the fractional polarizations. $1'$ corresponds to 20 %. Vectors are only plotted if $p \geq 3\,\%$. Coordinates are in B(1950.0)

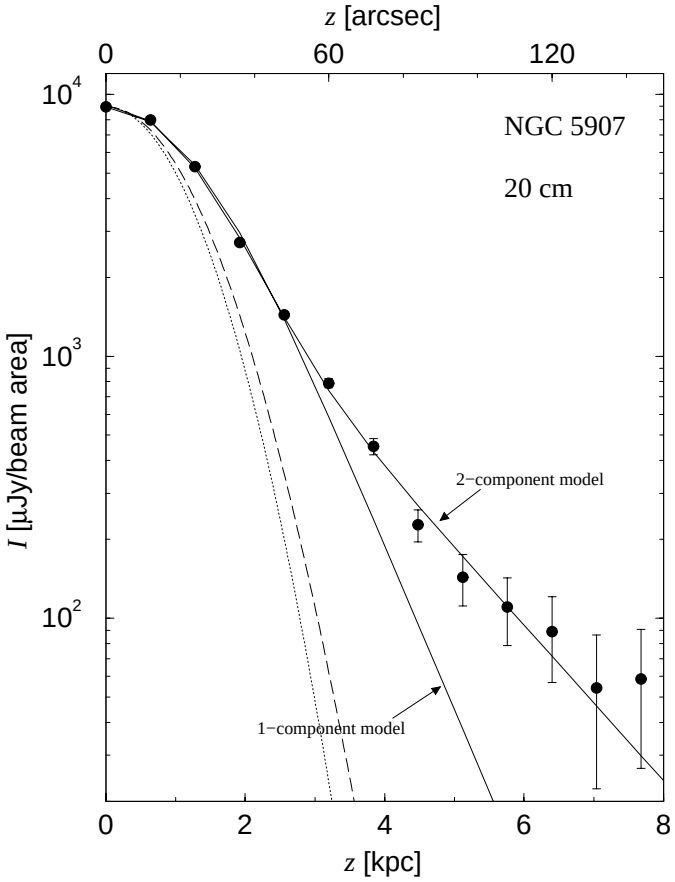

Fig. 6. Brightness distribution of the 20 cm emission of NGC 5907 perpendicular to the major axis (filled circles), at a resolution of $41''$ $HPBW$. Also shown are the beam (dotted line), the modelled distribution for an infinitely thin disk (dashed line), and the fitted distributions for a one- or two-component intrinsic distribution convolved with the beam (solid lines)

lent" have correlation lengths smaller than about 2 kpc, while the "large-scale" fields which are observable via linearly polarized emission are ordered on scales larger than about 8 kpc. Hence there is no continuous transition from small- to large-scale fields with increasing correlation lengths, but there may be rather two different field types which must be explained by models of magnetic field generation in galaxies.

At λ 2.8 cm we could not detect any significant polarized emission from NGC 5907. Taking the maximum polarized intensity at 6.2 cm (~ 0.6 mJy/beam) and an assumed synchrotron spectral index of $\alpha_{\mathrm{nt}} = -0.8$, we expect at 2.8 cm a polarized intensity of about 70 μJy/beam at a resolution of $69''$ ($HPBW$), which is clearly below the detection limit, even if we consider smaller depolarization effects than at 6.2 cm.

The preferred orientation of the observed ($E+90$)-vectors is *not* aligned along the galactic plane, but more or less in north-south direction. Foreground Faraday rotation cannot account for this deviation from a plane-parallel alignment at this wavelength. From the rotation measures of extragalactic sources observed by Simard-Normandin et al. (1981) we estimate a mean Faraday rotation measure in the direction of NGC 5907 (Galactic coordinates: $l \sim 92°; b \sim 52°$) of $RM_{\mathrm{fg}} = +7 \pm 7\,\mathrm{rad/m^2}$. At λ 6.2 cm this value leads to a rotation of the observed polarization vectors of only $\Delta\chi = 1\overset{\circ}{.}5 \pm 1\overset{\circ}{.}5$ which is negligible.

At 20 cm the situation is different. The foreground Faraday RM leads to a rotation of the polarization vectors of $16° \pm 16°$ at this wavelength. However, because of the large uncertainty, this rotation is difficult to take into account.

4. Analysis and discussion

4.1. Emission components

In order to examine the distribution of the radio continuum emission perpendicular to the major axis of NGC 5907, we performed a strip integration in the total intensity map at λ 20 cm (with $41''$ angular resolution, corresponding to about 2.2 kpc), centered on the position given in Table 1. This integration included the inner $300''$ along the major axis (but not the central $100''$) in order to yield a sufficiently high S/N-ratio and intensity values which represent statistically significant sample points for the disk of NGC 5907. The values for the northeastern and southwestern part of the galaxy were averaged.

The obtained intensity distribution of the radio continuum emission perpendicular to the major axis is shown in Fig. 6 (filled circles). We note here that even if the abscissa of Fig. 6 is labelled "*z* [kpc]" the curves do not really show the distribution perpendicular to the plane of the galaxy, but that perpendicular to the major axis projected onto the sky (the difference, however, may be negligible). In order to analyse the distribution quantitatively, we fitted the intensities with a model distribution consisting of an intrinsic one- or two-component exponential profile convolved with a Gaussian representing the CLEAN telescope beam. For an inclination of exactly 90° (perfect edge-on orientation) this Gaussian would have a width of $HPBW = 41''$. To correct approximatively for the inclination ($i = 86\overset{\circ}{.}5$) we used the width of an infinitely-thin-disk model instead. This was estimated by a fit to the major axis distribution, projected to the inclination angle, to be $44\overset{''}{.}3$. For the analytical form of the fitted profile see Dumke et al. (1995).

The functions thus obtained are shown for both cases (one or two components) as solid lines in Fig. 6, with the broader curve representing the fit from a two-component function. Obviously this model fits the data points much better than a single component. This is a clear evidence that the radio continuum emission of NGC 5907 at cm-wavelengths is composed of 2 components with different scale heights and probably also different spectral behaviour. We refer to the two components as "thin disk" and "thick disk" respectively. The exponential scale height found for the thin disk component is $z_{\rm e,thin} = 0.34\,{\rm kpc}$, its maximum intensity is $I_{0,\rm thin} = 22.08\,{\rm mJy/beam}$. For the thick disk component these values are $z_{\rm e,thick} = 1.5\,{\rm kpc}$ and $I_{0,\rm thick} = 3.84\,{\rm mJy/beam}$. These values are of the same order as found for other edge-on galaxies by Dumke & Krause (1998) at λ 6.2 cm. The scale height of the thick-disk component should, however, be rather taken as a lower limit, since the amount of lost flux of extended structures due to the missing spacings of the VLA is unknown (see also the spectral indices as a function of z in the next subsection).

Under the assumption that the scale heights of the two emission components do not change with radius, we can estimate the fraction of the total flux density $S_{20\rm cm}$ that is radiated from either component by integrating the generic functions of both components with z. We find ${\rm f_{thin}} \sim 58\,\%$ and ${\rm f_{thick}} \sim 42\,\%$. Of course these values are only valid at λ 20 cm, since we expect a different spectral behaviour of both components, due to a larger amount of thermal emission and a flatter energy distribution of the relativistic electrons in the thin disk.

At $\lambda\lambda$ 2.8 and 6.2 cm, the angular resolution is not sufficient to do a decomposition into a thin and thick disk component. A similar fit using only one emission component leads to a scale height of $\sim 1\,{\rm kpc}$ at 2.8 cm and $\sim 1.5\,{\rm kpc}$ at 6.2 cm.

4.2. Spectral indices and free-free-emission

After subtracting the two point sources in the southern half of NGC 5907, we can redetermine the total fluxes of the galaxy at the three wavelengths considered here and the corresponding spectral indices. The flux densities are $122 \pm 13\,{\rm mJy}$, $58\pm7\,{\rm mJy}$, and $41\pm6\,{\rm mJy}$ at wavelengths of 20, 6.2, and 2.8 cm respectively. Including the flux density values at 610 MHz given by Hummel et al. (1984), we find a spectral index in the long-wavelength range of $\alpha_{49/20} \sim -0.8$, but flatter spectra of $\alpha_{20/6.2} = -0.65$ and even $\alpha_{6.2/2.8} = -0.47$ at shorter wavelengths. These differences indicate the existence of a large amount of thermal free-free emission in this galaxy, as already suggested by Niklas et al. (1997).

We can use our data to estimate the fraction of thermal emission at each wavelength, making a least-squares-fit to the flux density values with the thermal and nonthermal contribution and the synchrotron spectral index $\alpha_{\rm nt}$ as free parameters, i.e. of the form

$$S_\nu = A\nu^{\alpha_{\rm nt}} + B\nu^{-0.1}\ . \qquad (1)$$

Using the data points at $\lambda\lambda$ 20, 6.2, and 2.8 cm, we find a nonthermal spectral index of $\alpha_{\rm nt} = -1.06$ and thermal fractions of 30 %, 55 %, and 73 % for the three wavelengths respectively. When we include the data point at 49 cm from Hummel et al. (1984), our fit leads to slightly different values of $\alpha_{\rm nt} = -0.91$ and thermal fractions which are about 20 % lower, which is still high compared to those usually expected for radio emission of galaxies in the cm-range. These values are, however, in agreement with the work of Niklas et al. (1997), who still may have underestimated the thermal fraction because of the contribution of the (steep-spectrum) point sources S1 and S2 (see previous section) to the total flux densities.

The thermal free-free emission might be even more important in the thin disk of the galaxy, where star formation occurs and where we observe a larger fraction of H II regions compared to the probably purely nonthermal emission at larger z-heights. Applying the strip integrations mentioned in the previous subsection to the data at 2.8 and 6.2 cm, we can determine the distribution of the spectral index as a function of distance from the major axis. This must be done at the same resolution for all wavelengths, so we smoothed the data at 20 and 2.8 cm to a beam of $147''$ ($HPBW$). The resulting distributions are shown in the upper panel of Fig. 7; the lower panel shows the z-distribution of the spectral indices between 20 and 6.2 as well as between 6.2 and 2.8 cm.

With increasing distance from the major axis of the galaxy there are two different phenomena which have an influence on the spectral index. First, the thermal fraction of the total emission is higher in the disk than above the disk, which may cause a steepening of the spectrum. This effect is expected to be stronger in the high-frequency range. Second, the relativistic electrons which produce the nonthermal synchrotron emission are expected to originate in the thin disk and to show a steeper energy distribution above the disk (due to particle aging). Both effects would lead to a steepening of the total spectral index α, with a stronger effect at high frequencies. This steepening is only observed between 6.2 and 2.8 cm, where both data sets come from a single-dish telescope. Between 20 and 6.2 cm the spectrum seems to flatten, but the most probable reason for this behaviour may be the fact that we lost extended flux with the interferometer observations at 20 cm. This effect is, however, negligible at

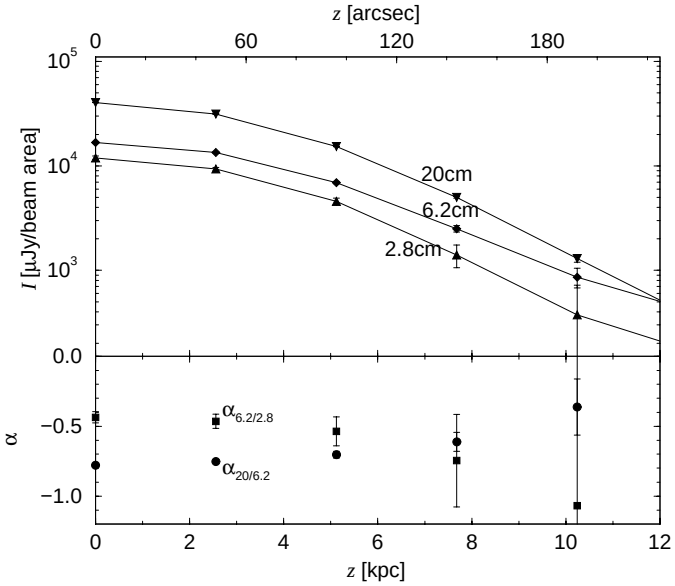

Fig. 7. Distribution of the radio continuum emission and the spectral indices perpendicular to the major axis of NGC 5907, at a linear resolution of $147''$ ($\widehat{=}$ 7.8 kpc)

$z = 0$ where the intensities are sufficiently high. Here, i.e. in the disk, we observe spectral indices of $\alpha_{20/6.2} \sim -0.78$ and $\alpha_{6.2/2.8} \sim -0.44$. This difference is consistent with a thermal fraction of about 60 % at 6.2 cm and even 80 % at 2.8 cm. Even with a refined emission model (Eq. 1) introducing a third spectral component (young relativistic electrons with $\alpha_{\rm SNR} = -0.5$ from adiabatic shock acceleration) the measured spectral indices yield lower limits for the fraction of thermal emission in the disk of $\mathrm{f_{th,20cm}} = 25\,\%$, $\mathrm{f_{th,6.2cm}} = 54\,\%$, and $\mathrm{f_{th,2.8cm}} = 70\,\%$ for the three observed wavelengths. We will use these values for the calculations in the following subsections.

These high values for the thermal (i.e. free-free) contribution to the total emission in the cm-range seem to contradict previous results on nearby galaxies, including face-on objects (e.g. Hummel et al. 1991; Neininger et al. 1993). There are two possible explanations. Since previous investigations of edge-on galaxies always tried to achieve the highest possible spatial resolution, they used interferometer data where the amount of lost flux, especially at high z or large radii, could only be roughly estimated, and the results may therefore have sometimes led to unreliable conclusions. For nearby face-on galaxies, on the other hand, the resolution of large single-dish telescopes may often be sufficient to perform a detailed study of these objects. But on average there is an inherent bias towards more luminous galaxies, because for face-on objects the emissivity must be much higher to be observed at similar intensities as edge-on galaxies, due to the shorter line-of-sight through the galaxy. Hence face-on galaxies may on average represent a different sample of objects, with different ISM properties. Additionally the amount of thermal gas in edge-on galaxies is more difficult or even impossible to estimate from Hα line emission because of the higher extinction in edge-on galaxies, which hinders a straightforward comparison of different tracers of thermal gas.

Fig. 8 shows the distribution of the radio continuum emission along the major axis of NGC 5907 at the three wavelengths as well as the spectral index distribution, at a resolution of $147''$. At all three wavelengths the distribution of the total emission is asymmetric. Whereas the emission at lower intensity levels is more extended to the south than to the north, which was already visible in the maps (Figs. 1 – 3), the maximum of the emission is shifted to the northern half. Hence it does not coincide with the optical and dynamical centre (which is determined by the total mass distribution). Since both free-free- and synchrotron radiation are consequences of star forming processes, these seem to occur at locally different levels. It is noteworthy that the molecular line and the cold dust emission which trace the raw material of star formation are distributed more or less symmetrically. However, the H I line emission is in general also a bit stronger in the northern half (Dumke et al. 1997).

There are also differences in the spectral indices between the northern and the southern half of this galaxy. Whereas the long-wavelength spectral index is more or less constant along the major axis ($\alpha_{20/6.2} \sim -0.78$), the spectral index between the two short wavelengths is flatter and asymmetric. In the southern half it is about -0.55, whereas in the northern half it reaches -0.1, which would mean that nearly all the emission is free-free radiation from H II regions. Even if the errors are large at larger radii, these very flat spectra occur in regions where we do not detect polarized emission at longer wavelengths. This may be a direct consequence of the thermal origin of a very large fraction of the emission (this means it is intrinsically unpolarized), but it may also point to stronger Faraday depolarization due to a larger thermal electron density and/or stronger (probably turbulent) magnetic fields.

4.3. Thermal electron densities

For a thermal fraction $\mathrm{f_{th}}(6.2\,\mathrm{cm}) = 54\,\%$ (see previous subsection) we determine for $z = 0$ a thermal radio flux density from H II regions of $S_{\rm th}(6.2\,\mathrm{cm}) = 9.1\,\mathrm{mJy}$ within one beam. We can then estimate the mean emission measure ($EM = \int n_{\rm e}^2\, dl$) following (e.g. Mezger & Henderson 1967)

$$\frac{EM}{\mathrm{pc\,cm^{-6}}} = \frac{4.13\, S_{\rm th}(\nu)}{\mathrm{mJy/beam}} \left(\frac{T_{\rm e}}{\mathrm{K}}\right)^{0.35} \left(\frac{\nu}{\mathrm{GHz}}\right)^{0.1} \left(\frac{\Theta}{'}\right)^{-2} \qquad (2)$$

with the electron temperature $T_{\rm e}$ and the half power beam width Θ. For an electron temperature of $T_{\rm e} = 10^4\,\mathrm{K}$ and a beam of $\Theta = 2\farcm45$ we find

$$EM = 190\,\mathrm{pc\,cm^{-6}}\ .$$

Since we observe at $z = 0$ also a fraction of the thick disk with our telescope beam of $2\farcm45$, we can expect this value to be a mixture of the thin- and thick-disk values. Taking into account that the thermal fraction of the emission at $z = 0$ would be much higher when observed with an appropriately small beam, we consider the value estimated above to be a lower limit to the thin disk itself.

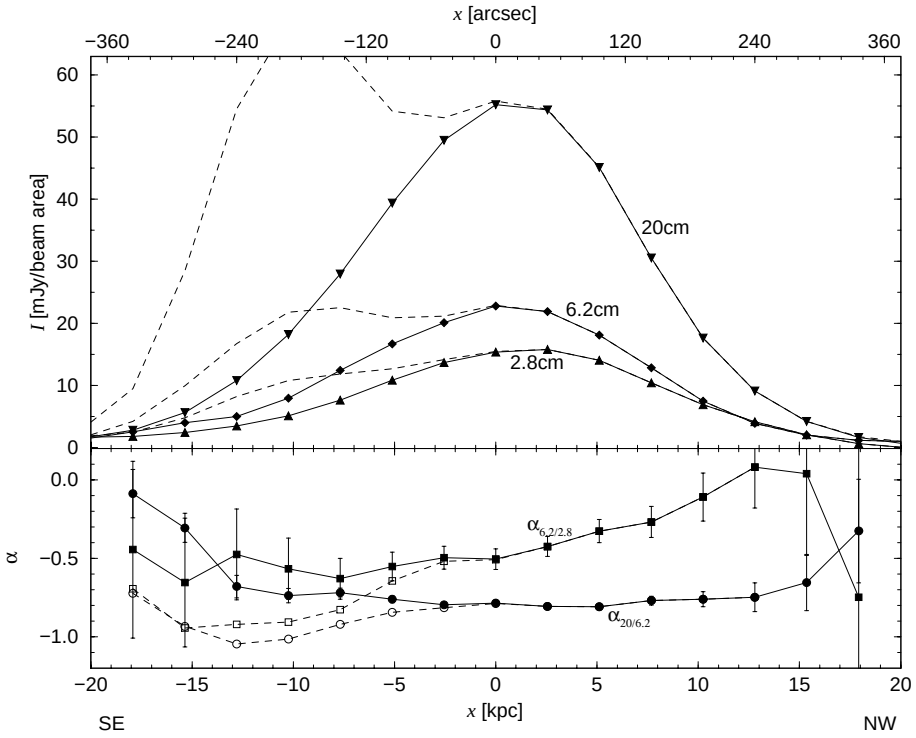

Fig. 8. Distribution of the radio continuum emission and the spectral indices along the major axis of NGC 5907, at a resolution of $147''$ ($\hat{=}$ 7.8 kpc). The dashed lines show the distributions prior to subtraction of the two point sources in the southern half

If we assume that the thermal electron density is constant along the line-of-sight, we can calculate it via

$$\langle n_\mathrm{e} \rangle = \sqrt{EM/(L\,f)}\,, \tag{3}$$

where L is the line-of-sight through the emitting medium and $f = \langle n_\mathrm{e}^2 \rangle / \langle n_\mathrm{e} \rangle^2$ a clumping factor that describes the variations of the electron density. For the local interstellar medium Manchester & Mebold (1977) found

$$f \sim 20\,.$$

If we assume that the thick-disk component is purely nonthermal, we can take for the line-of-sight L the projected thickness of the thin disk, for an inclination of $86\overset{\circ}{.}5$, i.e.

$$L = 2\,h_{\mathrm{thin\,disk}} / \cos i = 11.1\,\mathrm{kpc}\,.$$

We then find, using Eq. 3:

$$\langle n_\mathrm{e} \rangle = 0.03\,\mathrm{cm}^{-3}\,.$$

This value is the same as that derived by Lyne et al. (1985) for our galaxy. This means that the large fraction of thermal emission as discussed in the previous subsection is not the result of a high thermal electron density, but rather of a *deficit of nonthermal emission* – at least if we consider the thermal fractions estimated in previous studies to represent the "normal" case.

For the disks of 74 Shapley-Ames galaxies Niklas (1997) found that the ratio of non-thermal to thermal radio luminosity increases with increasing FIR luminosity, which means that galaxies with only a modest star-forming activity show a smaller amount of non-thermal emission relative to free-free radiation compared to more actively star-forming galaxies – a result which is consistent with our findings for NGC 5907.

4.4. Magnetic field strengths

Assuming energy equipartition between cosmic rays and the magnetic field, we can derive strengths for the total as well as for the large-scale ordered fields in the disk of NGC 5907, using the total and polarized intensities at $z = 0$. We use the $\lambda\,6.2$ cm data because we were able to detect polarized emission (in contrast to $\lambda\,2.8$ cm), while depolarization due to Faraday effects is not as strong as at longer wavelengths. Additionally the 6.2 cm data have the highest signal-to-noise ratio and therefore give the most reliable results. The method to estimate magnetic field strengths from the nonthermal radio emission was described in Krause et al. (1984) and further discussed by e.g. Beck (1991). To be consistent with previous publications we set the low-frequency spectral cut-off to $E_\mathrm{min} = 300\,\mathrm{MeV}$ particle energy and the ratio of the total energy density in cosmic rays to the electron energy density to $k = 100$. As length of the line-of-sight we choose $R_{25} = 19.7\,\mathrm{kpc}$, which seems an appropriate value considering the radial intensity profiles (Fig. 8).

With a nonthermal fraction of 46 % of the emission at $\lambda\,6.2$ cm, we derive a total magnetic field strength of $B_\mathrm{tot} = 5 \pm 1\,\mu\mathrm{G}$. For the large-scale uniform magnetic field we get from the polarized intensity a value of $B_\mathrm{u} \sim 1.1\,\mu\mathrm{G}$. While B_tot has a value similar to other galaxies, the strength of the uniform field B_u is smaller. This can have two possible reasons: the large-scale field may be intrinsically weak, or enhanced turbulence in the interstellar medium leads to significant depolarization, at least on the scale of the telescope beam. Since the main source of turbulence in the ISM is rapid star formation, and NGC 5907 shows only moderate star formation activity, the latter reason is rather unlikely in this case.

Table 3. Polarization angles and Faraday rotation measures towards selected regions of NGC 5907

	located at	$\chi_{18.0\mathrm{cm}}$	$\chi_{20.5\mathrm{cm}}$	RM [rad/m^2]
A	thin disk	$37^\circ \pm 11^\circ$	$68^\circ \pm 8^\circ$	56 ± 25
B	thin disk	$35^\circ \pm 5^\circ$	$70^\circ \pm 8^\circ$	63 ± 17
C	thick disk	$108^\circ \pm 8^\circ$	$120^\circ \pm 7^\circ$	22 ± 19
D	thick disk	$90^\circ \pm 10^\circ$	$98^\circ \pm 6^\circ$	15 ± 21
E	NGC5907-S2	$130^\circ \pm 3^\circ$	$106^\circ \pm 2^\circ$	282 ± 7 or -44 ± 7

If the large-scale field in NGC 5907 is intrinsically weak, the reason for this is unknown. Either the processes which create and/or amplify large-scale fields are less efficient in NGC 5907 than in other galaxies, or the field is somewhat younger and had not yet the time to increase to strengths like those in other galaxies.

4.5. Faraday rotation measures

Polarization data at more than one wavelength allow to estimate Faraday rotation measures (RMs) and therefore to investigate the strength and the orientation of ordered magnetic fields parallel to the line of sight. Unfortunately we were not able to detect polarized emission at λ 2.8 cm. We use instead the polarization maps at the two IFs around 20 cm. To this end we reduced the VLA data for the Stokes parameters U and Q with the same parameters as for the combined data set. Both IFs were tapered differently in the uv-plane to yield the same angular resolution. The resulting maps are shown in Fig. 9. Note that only the inner portion of Fig. 4 is shown here.

In order to analyse the magnetic field orientations quantitatively in terms of Faraday rotation and line-of-sight-parallel fields, we estimated the polarization angles for some selected regions of the galaxy, which are denoted by A – E in the 20.5 cm map. For these regions we determined Faraday rotation measures via

$$RM = \frac{\chi(\lambda_1) - \chi(\lambda_2)}{\lambda_1^2 - \lambda_2^2} \ , \tag{4}$$

where $\lambda_1 > \lambda_2$. For the two wavelengths the ambiguity of the rotation measure is $\pm 326\,\mathrm{rad/m^2}$. The results of these RM calculations are summarized in Table 3.

For the regions denoted A–D we find positive values for RM, indicating an ordered magnetic field directed *towards the observer*. We can also state that the rotation measures in the thick disk are substantially smaller than those in the thin disk which is easily explained by a smaller density of thermal electrons.

The interpretation of the result for region E is not as straightforward. First, we do not see polarized emission from the galaxy itself, but from the source NGC5907-S2, which is probably behind the galaxy, so that the pathlength through the Faraday-active medium is probably doubled. Second, the 2π ambiguity allows two reasonable values for RM. While $RM = 282\,\mathrm{rad\,m^{-2}}$ differs clearly from the values measured in the other regions in NGC 5907 (and may perhaps suggest another Faraday-active layer which has probably nothing to do with NGC 5907), the second possible value of $RM = -44\,\mathrm{rad\,m^{-2}}$ would support, if it is not intrinsic to the background source, a different direction of the line-of-sight-parallel magnetic field in this part of the galaxy. No final conclusion can be drawn here without high-resolution data at another wavelength.

When we use the RM values calculated above to estimate the E-field orientation for $\lambda = 0$, which is perpendicular to the unrotated (intrinsic) B-vectors, we find about -67° and -82° for the regions A and B respectively, but $+67^\circ$ and $+62^\circ$ for regions C and D respectively. The latter values suggest a plane-parallel field in the thick disk of NGC 5907, whereas in the thin disk we find a difference between major axis position angle and B-vector orientation of $30^\circ - 60^\circ$.

The RMs that we expect from the estimated thermal electron densities and magnetic field strengths can be calculated via

$$RM = 0.81 \int_0^{L/2} \frac{n_\mathrm{e}(l)}{\mathrm{cm^{-3}}} \frac{B_{\mathrm{u},\parallel}(l)}{\mu\mathrm{G}} \frac{dl}{\mathrm{pc}}\,\mathrm{rad\,m^{-2}} \ , \tag{5}$$

where $B_{\mathrm{u},\parallel}$ is the line-of-sight component of the uniform magnetic field (the parallel components of the turbulent field cancel on average). Under the assumption that n_e and $B_{\mathrm{u},\parallel}$ are constant along the line-of-sight, Eq. 5 simplifies to

$$RM = 0.81 \frac{\langle n_\mathrm{e} \rangle}{\mathrm{cm^{-3}}} \frac{B_{\parallel,\mathrm{eff}}}{\mu\mathrm{G}} \frac{L/2}{\mathrm{pc}}\,\mathrm{rad\,m^{-2}} \ , \tag{6}$$

with the effective parallel component $B_{\parallel,\mathrm{eff}}$ of the uniform field B_u. With some geometric considerations and assuming for simplicity a ring-like uniform field within the thin disk we get $B_{\parallel,\mathrm{eff}} \sim 0.66 \cdot B_\mathrm{u} \sim 0.73\,\mu\mathrm{G}$ (Dumke 1997), which leads to an expected rotation measure of

$$RM_\mathrm{exp} \sim 100\,\mathrm{rad\,m^{-2}} \ .$$

This value is somewhat larger than those estimated above for regions A and B. Even if the differences may already be explained by the uncertainties introduced by the assumptions we have made to estimate the values for n_e, B, and L, we suggest another explanation. Using

$$\Delta\chi = RM\,\lambda^2 - \chi(\lambda = 0) \ , \tag{7}$$

we find that an effective RM of $48\,\mathrm{rad\,m^{-2}}$ at λ 18.0 cm (and even $38\,\mathrm{rad\,m^{-2}}$ at λ 20.5 cm) is sufficient to completely depolarize the synchrotron radiation due to differential Faraday rotation (see Eq. 8). We conclude that the disk of NGC 5907 is not transparent to polarized emission at these wavelengths. The result is a reduction of the effective line-of-sight, because the radiation from the most distant parts of NGC 5907 is completely depolarized and only the Faraday rotation in the nearest parts of the disk can be measured by means of linearly polarized emission. A similar situation has already been observed in some face-on galaxies like M 51 (Horellou et al. 1992) or NGC 6946 (Ehle & Beck 1993). However, this means that the intrinsic B-field orientation cannot be determined from the observed RMs

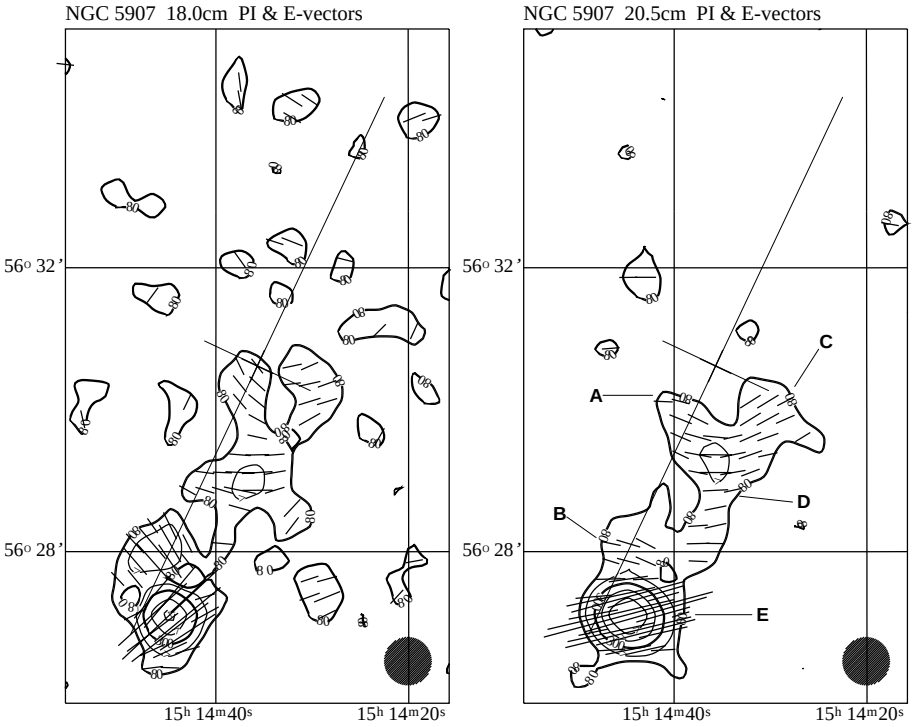

Fig. 9. Polarized intensities at 18 cm (left) and 20.5 cm (right). The $HPBW$ of $41''$ is indicated by the filled black circle in the lower right corner of each map. Contour levels are 80, 160, 300, 500, 700 μJy/beam. Vectors indicate the orientation of the *unrotated* E-vectors; their lengths are proportional to the polarized intensities. Vectors are only plotted for $PI \geq 100\,\mu$Jy/beam. The cross marks the centre and the major axis of the galaxy. Coordinates are in B(1950.0)

in the disk for $\lambda\,20$ cm. Using the value of $100\,\mathrm{rad\,m^{-2}}$ which was estimated from the thermal emission, we find a better agreement between major axis position angle and intrinsic B-field orientation, but we consider the uncertainties to be too large to yield reliable results in this case.

At $\lambda\,6.2$ cm the situation is more favourable. Here the estimated $RM_{\rm exp}$ would lead to a rotation of the polarization vectors of

$$\Delta\chi(6.2\,\mathrm{cm}) \sim 22^\circ\ ,$$

which is about the difference between the position angle of NGC 5907 and the observed B-field orientation. In other words: if the large-scale magnetic field is parallel to the disk, as it is in most other edge-on galaxies (e.g. Dumke et al. 1995), then the observed polarization angles can be explained by the expected Faraday rotation caused by the uniform magnetic field and the thermal electron densities that follow from the measured intensities and spectral index distributions.

4.6. Depolarization

As already mentioned, the emission at $\lambda\,6.2$ cm and especially at $\lambda\,20$ cm is partially depolarized by magnetic fields and thermal electrons along the line-of-sight in the disk of NGC 5907. In general, the depolarization mechanisms can be split into an instrumental part (basically beam depolarization), and an astronomical part, which consists of Faraday dispersion ($DP_{\rm disp}$) and differential Faraday rotation ($DP_{\rm diff}$). The latter is dependent on the large-scale magnetic field component along the line-of-sight, and is given by (Burn 1966):

$$DP_{\rm diff} = \left| \frac{\sin(2\,RM\,\lambda^2)}{2\,RM\,\lambda^2} \right| \ , \tag{8}$$

with the rotation measure RM determined by Eq. 5. Using $RM \sim 100\,\mathrm{rad\,m^{-2}}$ estimated in the previous subsection, we calculate $DP_{\rm diff,6.2cm} \sim 0.90$ at $\lambda\,6.2$ cm. At $\lambda\,20$ cm we would expect a much stronger depolarization ($DP_{\rm diff,20cm} \leq 0.1$), making the plane of the galaxy optically thick for linearly polarized emission, as already noted.

The so-called Faraday dispersion is a result of turbulent (or random) magnetic fields and thermal electrons in the emitting regions and can be described by (Burn 1966):

$$DP_{\rm disp} = \frac{1 - \mathrm{e}^{-\sigma_{RM}\lambda^4}}{\sigma_{RM}\lambda^4}\ , \tag{9}$$

where σ_{RM} is the variance of rotation measure

$$\sigma_{RM} = \left(0.81\,\frac{n_{\rm e}}{\mathrm{cm^{-3}}}\,\frac{B_{\rm r}}{\mu\mathrm{G}}\right)^2 \frac{d}{\mathrm{pc}}\,\frac{L}{\mathrm{pc}}\,\mathrm{rad^2 m^{-4}}\ . \tag{10}$$

Here $B_{\rm r}$ is the random component of the total magnetic field $B_{\rm tot}$, d the typical size of a turbulence cell of the random magnetic field (or the "correlation length"), and L the line-of-sight through the Faraday active medium. Following results from our Galaxy, we assume a typical correlation length for the turbulent magnetic field of $d = 55\,\mathrm{pc}$ (Rand & Kulkarni 1989). With a random magnetic field of

$$B_{\rm r} = \sqrt{B_{\rm tot}^2 - B_{\rm u}^2} = 4.9\,\mu\mathrm{G}$$

we find $\sigma_{RM} \sim 8700\,\mathrm{rad^2 m^{-4}}$, hence a depolarization of $DP_{\rm disp,6.2cm} \sim 0.94$ at $\lambda\,6.2$ cm. Even if we assume larger correlation lengths, the depolarization due to Faraday dispersion is not much smaller and cannot account for the observed fractional depolarization. Around $\lambda\,20$ cm, on the other hand,

we expect this effect to be also much stronger and to yield a depolarization of $DP_{\rm disp,20cm} \leq 0.1$.

Taking these depolarization effects at $\lambda\,20$ cm into account, the observed polarization in the southwestern part of NGC 5907 can only be explained when we assume that the large-scale magnetic field responsible for this polarized emission is located in the front part of the galaxy. The asymmetry of the polarization pattern with respect to the major axis in the southern half (see Figs. 1, 4, and 9) may simply be explained by the orientation of NGC 5907 in space: the eastern half represents the rear part of this galaxy. In the northwestern half of the disk this is also true, but note that the fraction of the (intrinsically unpolarized) thermal emission is much larger there (see Fig. 8).

At $\lambda\,6.2$ cm, where the astronomical (Faraday) depolarization effects are much weaker, the small observed degree of polarization is due to larger beam depolarization, and also to the larger thermal fraction of the emission, as argued in Sect. 4.2.

5. Summary and conclusions

We have observed the total and linearly polarized radio continuum emission of the large nearby edge-on galaxy NGC 5907 at wavelengths of 20, 6.2, and 2.8 cm. After subtraction of a double background source with a steep spectrum ($\alpha < -1$) the total power maps show a maximum intensity slightly shifted to the north with respect to the optical and dynamical centre at all wavelengths.

The emission perpendicular to the plane could be explained by two emission components: a thin and a thick disk with exponential scale heights of 0.34 kpc and 1.5 kpc respectively at 20 cm, with the thin disk containing about 58 % of the total flux density at this wavelength.

From an analysis of the total power data we found that the integrated spectrum of the galaxy can best be described as a mixture of nonthermal (synchrotron) and thermal (free-free) emission, with the latter contributing a surprisingly large fraction ($> 50\,\%$) of the total flux densities in the cm range. This fraction is even larger *in the disk* of NGC 5907, when we analyse the emission of the thin and thick disk separately. The influence of (unpolarized) thermal emission for the total emission is further supported by a local correlation between flat spectra (up to $\alpha \sim -0.1$) and low fractional polarization. We calculated average thermal electron densities of $n_{\rm e} \sim 0.03\,{\rm cm}^{-3}$ for the thin disk, a value similar to the local interstellar medium. Hence we conclude that the large thermal fraction does not indicate enhanced thermal emission, but rather a deficit of nonthermal emission, which is probably a direct consequence of the modest star formation activity of NGC 5907.

From the nonthermal and the polarized intensity along the major axis at $\lambda\,6.2$ cm we estimate the total magnetic field strength in NGC 5907 to be $B_{\rm tot} \sim 5\,\mu$G, a value similar to other galaxies. The strength of the large-scale field, $B_{\rm u} \sim 1.1\,\mu$G, is, however, relatively weak. This weakness, together with the small amount of nonthermal emission at high frequencies, can easily explain the non-detection of polarized emission at $\lambda\,2.8$ cm.

The morphology of the observed polarized emission at $\lambda\,20$ cm exhibits an asymmetry with respect to the major axis. Only the southwestern half shows significant polarization, which can be explained by the emission from the rear eastern side passing through a Faraday-active (depolarizing) medium within the disk of the galaxy. The observed asymmetry *along* the major axis with respect to the centre is most probably due to the larger fraction of thermal emission in the nothern half. With our estimated electron densities and magnetic field strengths, the observed polarization angles at $\lambda\,6.2$ cm are consistent with a large-scale magnetic field parallel to the disk of NGC 5907, as observed in most other edge-on galaxies.

When we compare our results with previous ones on the radio continuum emission in nearby galaxies, we argue that in general a higher star formation activity, as observed in some other galaxies, may lead to a proportional enhancement of the thermal free-free emission from H II regions, but – with some time lag – to a much more significant increase of the number density of relativistic electrons and a more effective amplification of the large-scale magnetic field. This leads to a higher amount of nonthermal (synchrotron) radiation from those more actively star forming galaxies than from the rather inactive galaxy NGC 5907.

References

Barnaby D., Thronson H.A. Jr., 1992, AJ 103, 41
Beck R., 1991, A&A 251, 15
Burn B.J., 1966, MNRAS 133, 67
de Vaucouleurs G., de Vaucouleurs A., Corwin H.G., et al., 1991, Third Reference Catalogue of Bright Galaxies. Springer-Verlag, New York
Dumke M., 1997, Ph.D. Thesis, University of Bonn
Dumke M., Krause M., 1998, In: Breitschwerdt D., Freyberg M., Trümper J. (eds.) Proc. IAU Coll. 166, The Local Bubble And Beyond. Lecture Notes in Physics 506, Springer-Verlag, Berlin, p. 555
Dumke M., Krause M., Wielebinski R., Klein U., 1995, A&A 302, 691
Dumke M., Braine J., Krause M., et al., 1997, A&A 325, 124
Ehle M., Beck R., 1993, A&A 273, 45
Emerson D.T., Gräve R., 1988, A&A 190, 353
Emerson D.T., Klein U., Haslam C.G.T., 1979, A&A 76, 92
García-Burillo S., Guélin M., Neininger N., 1997, A&A 319, 450
Guélin M., Sancisi R., Weliachew L., van Woerden H., 1974, In: Weliachew L. (ed.) La Dynamique des Galaxies Spirales. 291. Colloque C.N.R.S., Editions du CNRS, p. 241
Horellou C., Beck R., Berkhuijsen E.M., Krause M., Klein U., 1992, A&A 265, 417
Hummel E., Sancisi R., Ekers R.D., 1984, A&A 133, 1
Hummel E., Dahlem M., van der Hulst J.M., Sukumar S., 1991, A&A 246, 10
Krause M., Beck R., Klein U., 1984, A&A 138, 385
Lequeux J., Fort B., Dantel-Fort M., Cuillandre J.-C., Mellier Y., 1996, A&A 312, L1
Lequeux J., Combes F., Dantel-Fort M., et al., 1998, A&A 334, L9
Lyne A.G., Manchester R.N., Taylor J.H., 1985, MNRAS 213, 613
Manchester R.N., Mebold U., 1977, A&A 59, 401
Mezger P.G., Henderson A.P., 1967, ApJ 147, 471

Neininger N., Beck R., Sukumar S., Allen R.J., 1993, A&A 274, 687
Niklas S., 1997, A&A 322, 29
Niklas S., Klein U., Wielebinski R., 1997, A&A 322, 19
Rand R.J., Kulkarni S.R., 1989, ApJ 343, 760
Rottmann H., 1996, Diploma Thesis, University of Bonn
Rottmann H., Mack K.-H., Klein U., Wielebinski R., 1996, A&A 309, L19
Sackett P.D., Morrison H.L., Harding P., Boroson T.A., 1994, Nat 370, 441
Sancisi R., 1976, A&A 53, 159
Sasaki T., 1987, PASJ 39, 849
Shang Z., Zheng Z., Brinks E., et al., 1998, ApJ 504, L23
Simard-Normandin M., Kronberg P.P., Button S., 1981, ApJS 45, 97
Young J.S., Xie S., Kenney J.D.P., Rice W.L., 1989, ApJS 70, 699